

# Laboratoire de l'Accélérateur Linéaire

## POSITRON SOURCES

Robert CHEHAB

*Lecture given at the CERN Accelerator School,  
19 - 30 September 1988, Salamanca, Spain*

U.E.R  
de  
l'Université Paris-Sud



Institut National  
de Physique Nucléaire  
et  
de Physique des Particules

Bâtiment 200 - 91405 ORSAY Cedex

## POSITRON SOURCES

R. Chehab

Laboratoire de l'Accélérateur Linéaire, Orsay, France

### ABSTRACT

A tentative survey of positron sources is given. Physical processes on which positron generation is based are indicated and analyzed. Explanation of the general features of electromagnetic interactions and nuclear  $\beta^+$  decay makes it possible to predict the yield and emittance for a given optical matching system between the positron source and the accelerator. Some kinds of matching systems commonly used – mainly working with solenoidal fields – are studied and the acceptance volume calculated. Such knowledge is helpful in comparing different matching systems. Since for large machines, a significant distance exists between the positron source and the experimental facility, positron emittance has to be preserved during beam transfer over large distances and methods used for that purpose are indicated. Comparison of existing positron sources leads to extrapolation to sources for future linear colliders.

### INTRODUCTION

In recent years, there has been increasing interest in the use of high intensity positron beams in storage and collider rings. With the advent of linear colliders such as SLC or others presently under study, more stringent conditions are imposed on positron intensity and emittance.

Positron beam intensity and emittance are strongly related to the methods of production and collection. Positron generation by electromagnetic interactions or nuclear  $\beta^+$  decay present different features which will be analyzed. Thermic processes in the target have also to be considered. However, knowledge of the positron production rate is insufficient to calculate the actual beam intensity which is also dependent on collection devices and, obviously, on linac acceptance. Positron emittance is mainly determined by the converter and the matching system. Very often, longitudinal ( $\Delta\phi$ ,  $\Delta E/E$ ) and transverse ( $x$ ,  $x'$ ;  $y$ ,  $y'$ ) emittances have to be reduced to deal with storage ring injection requirements or linear collider interaction point conditions. Beam transport and trajectory control are of particular importance in ensuring that the intensity and emittance of the beam are protected from the effects of wake fields. Some comparisons between existing  $e^+$  sources will lead to predictions of yields, emittance and the feasibility of positron sources for linear colliders.

#### 1. PHYSICAL PROCESSES ASSOCIATED WITH POSITRON PRODUCTION

Two kinds of physical processes lead to positron production : the electromagnetic interaction of a photon with the Coulomb field of the nucleus with consequent pair production, and the weak interaction occurring in nuclear  $\beta^+$  decay.

##### 1.1. Electromagnetic interaction [1]

Charged particles traversing a target lose energy by radiation and collision. The energy lost by collision is used in atom excitation and ionization leading to secondary electron emission and is hence essentially dissipated. This represents the main contribution to heating processes in the target. The energy lost by radiation

– Bremsstrahlung – is distributed among the secondary photons whose energy can reach the primary electron energy. The created photons interacting with the nucleus, and in a weaker manner with the peripheral electrons, undergo materialization with subsequent pair creation. The Compton effect could also occur by elastic collision of the photons with electrons. The electron pairs radiate photons and are then transformed into other pairs, the energy of the created electrons decreasing at each step. Such a process is called a **cascade shower** (Fig. 1). Electromagnetic showers can be initiated by high energy photons as well as by high energy electrons.

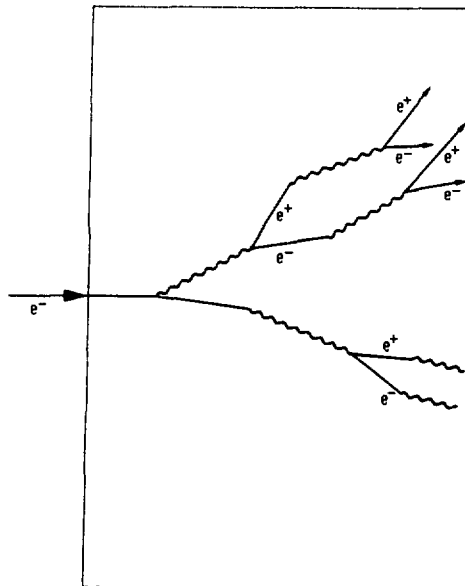


Fig. 1 Electron generated cascade shower

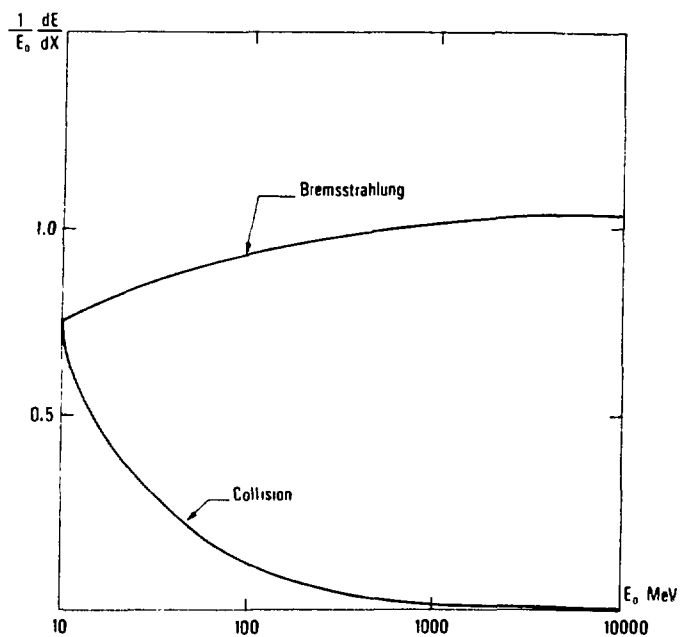


Fig. 2 Fractional energy losses by collision and Bremsstrahlung  
(from B. Rossi, ref. 1)

Bremsstrahlung, pair creation, ionization and Compton effect are not the only processes encountered. Among others, multiple Coulomb scattering is of some importance since it mainly determines the lateral spread of the shower. The relative importance of these various phenomena may be examined by comparing their cross sections. We present in Fig. 2 the losses by Bremsstrahlung and collision processes. For positron production, pair materialization of photons - directly impinging on the target or radiated by the incident electrons - is the essential phenomenon. The Bremsstrahlung differential cross section is given by [2] :

$$\frac{d\sigma_{\text{Brem}}(Z, E_0, k)}{dk} = \frac{A'(Z, E_0) r_e^2 \alpha Z(Z + \xi(Z))}{k} \times \left\{ \left( 1 + (E/E_0)^2 \right) \right. \quad (1.1)$$

$$\left. \left[ \phi_1(\delta) - \frac{4}{3} \ln Z - (4 f_c(Z) \text{ if } E_0 > 50, 0) \right] - \frac{2}{3} (E/E_0) \left[ \phi_2(\delta) - \frac{4}{3} \ln Z - (4 f_c(Z) \text{ if } E_0 > 50, 0) \right] \right\}$$

where  $E_0$  is the incident electron energy in MeV

$\alpha = 1/137$

$r_e$ , electron classical radius

$k$ , photon energy in MeV

$E$ , electron energy in MeV

$Z$ , target material atomic number

$$\delta = \frac{136}{Z^{1/3}} \cdot \frac{km}{E_0 E}$$

$\phi_1(\delta)$  and  $\phi_2(\delta)$  are the screening functions

$f_c(Z)$  is the coulomb correction term (Davies, Bethe, Maximon)

$m$  is the electron rest energy in MeV.

The pair production cross section is given by :

$$\frac{d\sigma_{\text{pair}}(Z, k, E_+)}{dE_+} = \frac{A'_p(Z, k) r_e^2 \alpha Z(Z + \xi(Z))}{k^3} \times \left\{ \left( E_+^2 + E_-^2 \right) \right. \quad (1.2)$$

$$\left. \left[ \phi_1(\delta) - \frac{4}{3} \ln Z - (4 f_c(Z) \text{ if } k > 50, 0) \right] + \frac{2}{3} E_+ E_- \left[ \phi_2(\delta) - \frac{4}{3} \ln Z - (4 f_c(Z) \text{ if } k > 50, 0) \right] \right\}$$

where  $E_+$  and  $E_-$  are the positron and electron energies respectively

$$\xi = \ln(1440 Z^{-2/3}) / \ln(183 Z^{-1/3})$$

$$\delta = \frac{136}{Z^{1/3}} \cdot \frac{k \cdot m}{E_+ E_-}$$

We may notice that Bremsstrahlung and pair production cross sections are a rapidly increasing function of the material's atomic number. For this reason tungsten (74) and tantalum (73) are good candidates for positron converters.

### 1.1.1 *Some methods for shower analysis*

Analytical as well as numerical analysis have been extensively used to study positron generation.

### Analytical approaches

Since angles of emission of secondary electrons and photons at high energies are quite small in low Z elements, the electron scattering is also small and the electromagnetic cascade shower is developed in the direction of the incident particle. This allows the longitudinal shower development and the lateral spread to be treated as two separate problems. For higher Z materials this assumption remains valid only for the more energetic secondary particles. Nevertheless, it constitutes a convenient approach and the following approximations can be built on this basis :

- A) considers only Bremsstrahlung and pair creation.
- B) improves the former taking into account the ionization losses at a constant rate, and
- C) uses more precise cross section evaluations regarding B and takes into account the Compton effect [1].

Two quantities are relevant to positron production in the longitudinal direction : the position of the shower maximum and the number of secondary particles ( $e^+$  and  $e^-$ ) at this maximum. Both are derived using approximation B.

The position of the shower maximum is given by [1] :

$$T_{\max}^{e^-} = 1.01 [\ln (E_0/\epsilon_0) - 1] \quad (1.3)$$

for a primary electron

where  $E_0$  is the incident electron energy

$\epsilon_0$ , the material critical energy (energy at which radiation losses and collision losses are almost identical),

and

$$T_{\max}^{\gamma} = 1.01 \left[ \ln (E_0/\epsilon_0) - \frac{1}{2} \right] \quad (1.4)$$

for a primary photon.

The number of secondary particles at shower maximum is given by [1] :

$$\Pi_{\max}^{e^-} = \frac{0.31}{\left[ \ln (E_0/\epsilon_0) - 0.37 \right]^{1/2}} \cdot \frac{E_0}{\epsilon_0} \quad (1.5)$$

for a primary electron, and

$$\Pi_{\max}^{\gamma} = \frac{0.31}{\left[ \ln (E_0/\epsilon_0) - 0.18 \right]^{1/2}} \cdot \frac{E_0}{\epsilon_0} \quad (1.6)$$

for a primary photon.

These formulas clearly show the importance of using high energy incident particles. However, they give values which are too optimistic (see Fig. 3 and 4) compared with more exact calculations and especially the Monte-Carlo simulations by Crawford and Messel [3-4].

Most of the lateral spread features are due to multiple scattering. If we consider a parallel and infinitely narrow beam of particles impinging on a thin plate - so as to neglect the energy losses - we can describe the distribution of the secondary particles (in the  $y - \theta_y$  plane) by the Fermi function [1] :

$$P(z,y,\theta_y) dy d\theta_y = \frac{2\sqrt{3}}{\pi} \cdot \frac{1}{\theta_s^2 z^2} \exp \left\{ -\frac{4}{\theta_s^2} \left( \frac{\theta_y^2}{z} - \frac{3y\theta_y}{z^2} + \frac{3y^2}{z^3} \right) \right\} \quad (1.7)$$

where  $\theta_s^2$  represents the mean square angle of scattering defined by :

$$\theta_s = \frac{15}{E} \sqrt{\frac{z}{X_0}}$$

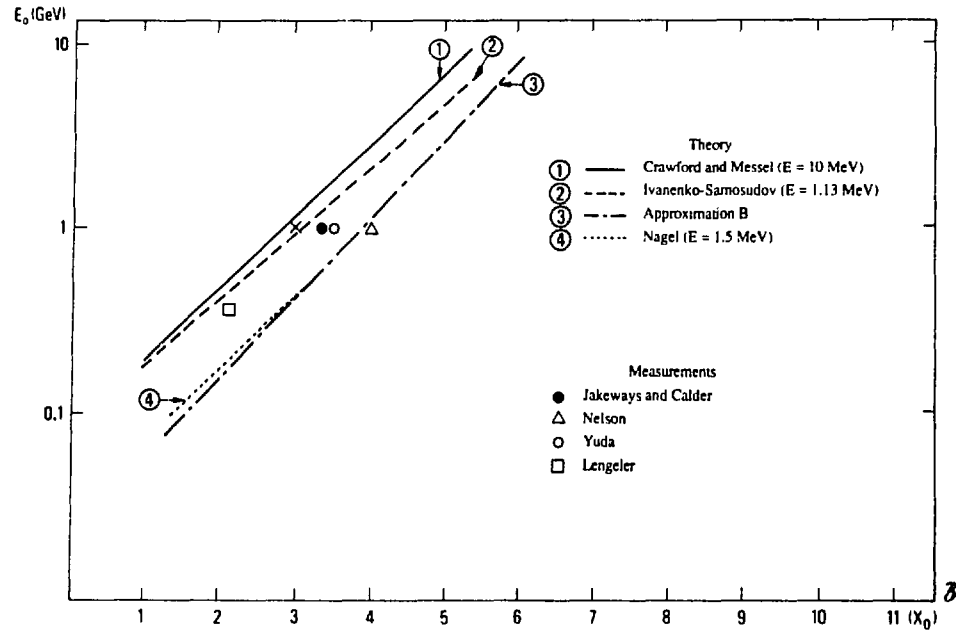


Fig. 3 Shower maximum position variation with incident energy (lead)  
Cut-off energy E is indicated (from R. Chehab, ref. 4)

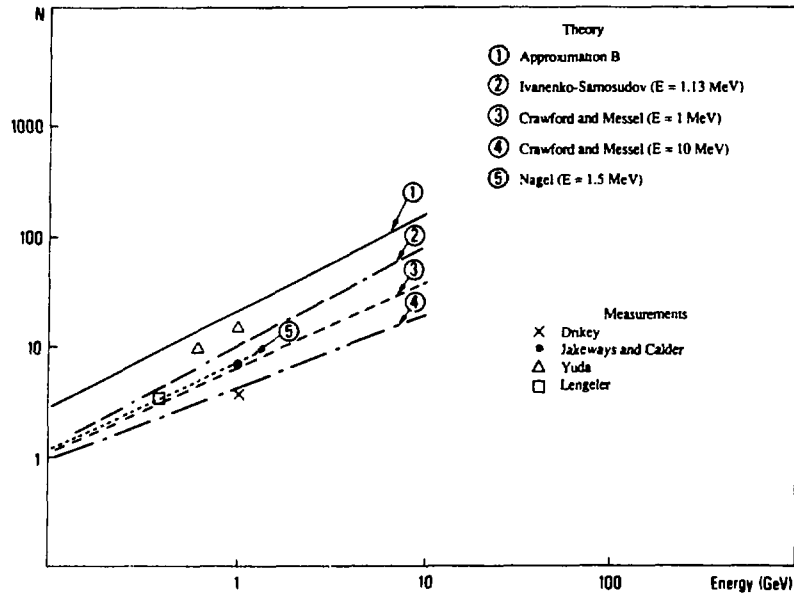


Fig. 4 Number of secondary particles at shower maximum (lead)  
Cut-off energy E is indicated (From R. Chehab, ref. 4)

### Monte Carlo simulation

When considering transport by magnetic lenses of positrons collected from the source, we are concerned with low energy positrons (some MeV). Moreover, use of high Z materials to improve pair creation leads to important electron scattering and hence to the lengthening of the particle path. Longitudinal development and lateral spread can no longer be separated. Monte Carlo calculations provide a more consistent approach to the problem due to more precise and complete analysis and from these Crawford and Messel tables [3] and EGS code [2] provide a good description of the problem. We shall use here mainly EGS results for a positron source excited by an electron or a photon beam.

We may characterize a positron source by its density  $\frac{d^3n}{dE dr d\Omega}$  where E, r and  $\Omega$  represent respectively the energy, radial distance to the axis and solid angle of emission of the emitted positron. Such a density may be determined at the converter exit using EGS code. To calculate the optimum thickness of the converter, we make use of the "Transition curve" (Fig. 5) which gives the variation of the number of secondary particles with the penetration depth of the material.

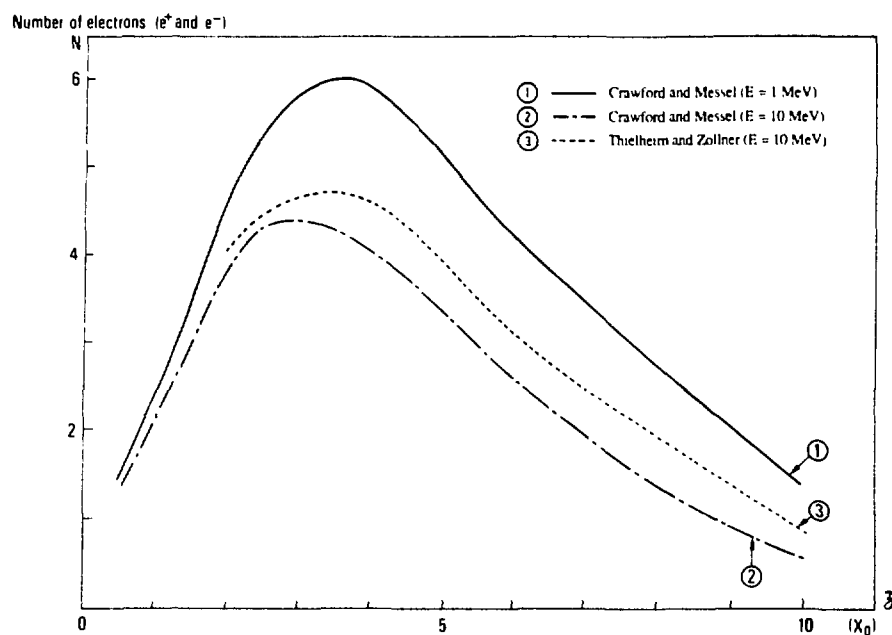


Fig. 5 Transition curve for 1 GeV incident electron (lead)  
Cutt-off energy E is indicated (from R. Chehab, ref.4)

Positron density and, more generally, positron emittance in the six-dimensional phase space  $\left[ x, \frac{dx}{dz}; y, \frac{dy}{dz}; \Delta\phi, \Delta E \right]$  may be represented – in a restrictive manner – by the following curves :

- Positron energy spectrum (Fig. 6)
- Radial distribution (Fig. 7)
- Angular distribution (Fig. 8).

Given an acceptance volume v defined by the limits :

$$\left[ (E_{\min}, E_{\max}); r_{\max}; \theta_{\max} \right],$$

we can write for the positron yield

$$n^+ = n_0 \iiint_v \frac{d^3 n}{dE dr d\Omega} dE dr d\Omega \quad (1.8)$$

where  $n_0$  is the total number of positrons produced by one incident electron or photon and  $d\Omega$  is the elementary solid angle defined by:

$$d\Omega = 2\pi \sin\theta d\theta.$$

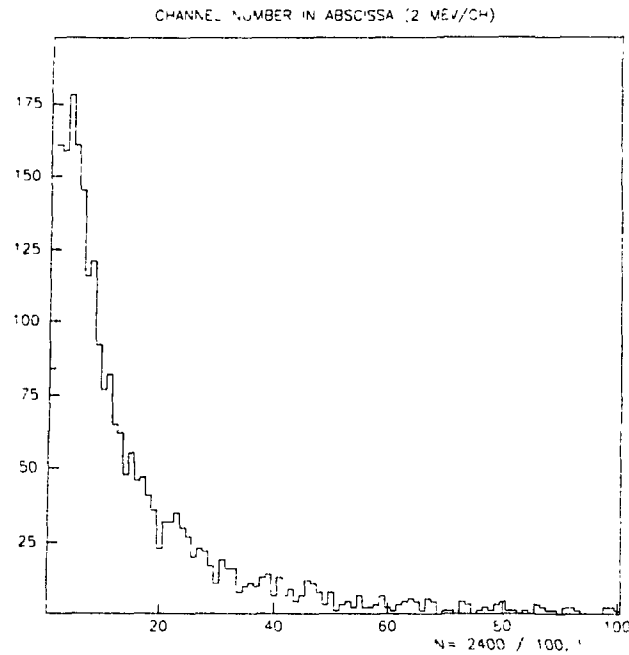


Fig. 6 Positron energy spectrum

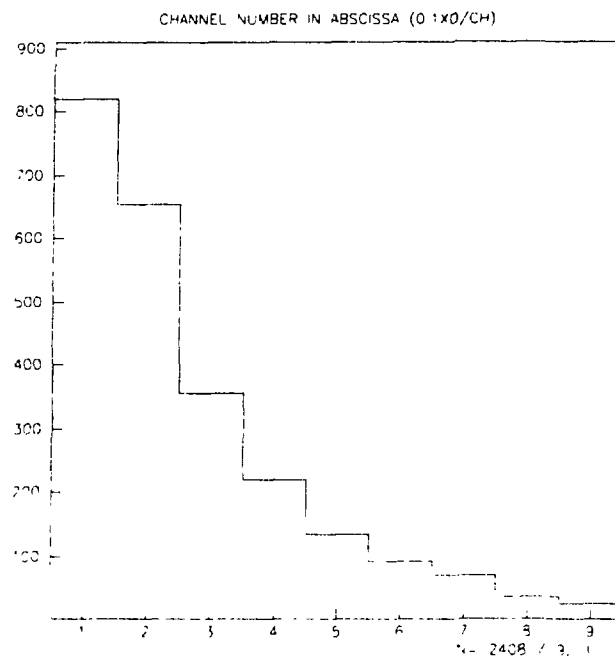


Fig. 7 Positron radial distribution

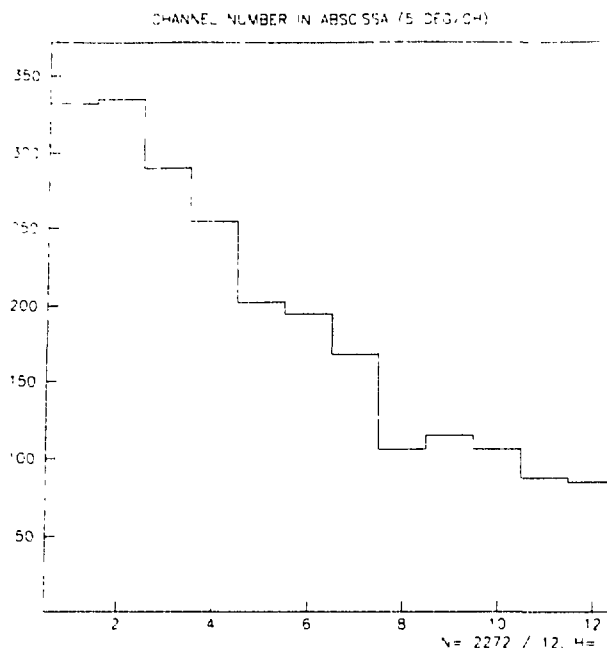


Fig. 8 Positron angular distribution

Such an expression can also be written as :

$$n_+ = n_0 \int_{E_{\min}}^{E_{\max}} \int_0^{r_{\max}} \int_0^{\theta_{\max}} f_E(E) f_r(r,E) f_{\theta}(\theta,E) 2\pi \sin\theta \, d\theta \, dr \, dE \quad (1.9)$$

where  $f_E$ ,  $f_r$ ,  $f_{\theta}$  are the distribution functions which can be derived from EGS simulations.

Nota : A more appropriate calculation should take into account the distribution in transverse momentum – which can be derived from EGS – instead of the angular distribution.

### 1.1.2 Thermic processes and radiation problems

Energy losses by ionization lead to thermal heating of the target while photons as well as secondary particles ( $e^+$  and  $e^-$ ) created in the target and not collected by the optical system produce a large amount of radiation.

#### Thermal heating

The thermic behaviour of the converter depends upon the electron beam intensity, dimensions, pulse width and repetition rate as well as the physical properties of the material. A basic quantity is represented by the fractional energy absorption per  $\text{cm}^3$   $\frac{1}{E_0} \cdot \frac{dE(r,z)}{dv}$  which can be obtained from shower codes such as EGS. We can also use the energy deposition per unit length in the target :  $\frac{1}{E_0} \cdot \frac{dE}{dz}$  where  $E_0$  is the incident electron energy. In Fig. 9, we show an example for this last quantity calculated for a tungsten target receiving a 2 GeV electron beam. We notice that most of the energy is deposited in the last fraction of the converter.

The pulse temperature rise is given by :

$$\Delta t_p = \frac{N E_0}{\rho C_p} \cdot \frac{1}{E_0} \cdot \frac{dE}{dv} \quad (1.10)$$

where  $\rho$  is the material density  
 $C_p$  its heat capacity  
 $N$  is the number of particles per pulse.

For a given peak intensity, this quantity grows linearly with the pulse width and inversely as the square of the beam diameter.

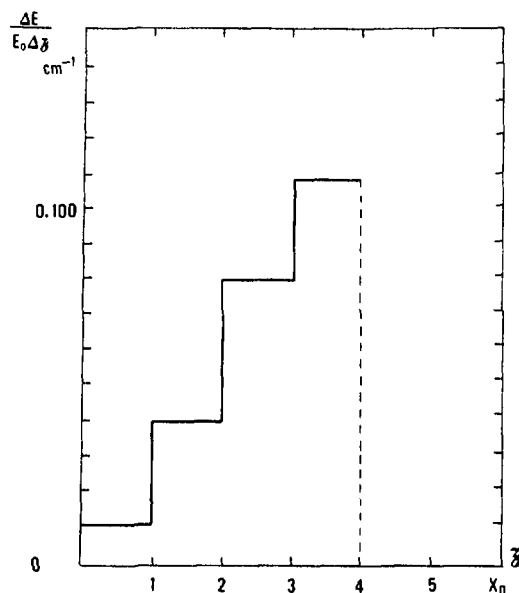


Fig. 9 Fractional energy absorption per unit length for 2 GeV electron

For a target of cylindrical geometry, the steady state temperature rise is given by [5] :

$$\dot{Q}(r) = v N E_0 \int_0^r \frac{1}{E} \frac{dE}{dv} 2\pi r dr = k_t 2\pi r \frac{dT}{dr} \quad (1.11)$$

where  $v$  is the pulse repetition rate  
 $k_t$  is the thermal conductivity.

$\frac{1}{E} \frac{dE}{dv}$  may be smoothed with a regular function and the expression (1.11) easily integrated.

Fatigue of the material may arise from stresses caused by thermal pulses. For a disk heated symmetrically about its centre, and uniformly throughout its thickness, the stresses are given as functions of the radius by [6] :

$$\sigma_{r1} = \tau E_y \left( \frac{1}{R^2} \int_0^R T(r) r dr - \frac{1}{r_1^2} \int_0^{r_1} T(r) r dr \right) \quad (1.12)$$

$$\sigma_{t1} = \tau E_y \left( -T(r) + \frac{1}{R^2} \int_0^R T(r) r dr + \frac{1}{r_1^2} \int_0^{r_1} T(r) r dr \right)$$

where  $R$  is the disk radius

$T(r)$  is the temperature at any point a distance  $r$  from the centre, minus the temperature of the coldest part of the disk

$\tau$  is the coefficient of thermal expansion

$E_y$  is the Young modulus.

For  $T(r)$ , we can take the pulse temperature rise  $\Delta t_p$ . In the expression (1.10), the quantity  $\frac{1}{E_0} \cdot \frac{dE}{dv}$  is a decreasing function of  $r$  and, therefore, also  $\Delta t_p$ . Thus the maximum stresses (at the hot central core) are given by :

$$\sigma_r = \sigma_t = -\frac{\tau E_y \Delta t_p (0)}{2(1 - \nu_p)} \quad (1.13)$$

where  $\nu_p$  is the Poisson Ratio (0.25 + 0.30).

### Radiation problems

In addition to the thermic problems, the large amount of radiation produced in the vicinity of the target constitutes one of the main difficulties of the classical positron sources. It leads to induced radioactivity in surrounding components, cooling water and air [7]. Radionuclides in the target, its metallic support (copper), the cooling water and the air are to be considered. Moreover, ozone formation increases with the beam power. Thus adequate shielding and efficient ventilation must be provided in the vicinity of the target.

### 1.2 Nuclear $\beta^+$ decay [8]

Most of the radioactive positron sources make use of (pn) or (n $\gamma$ ) reactions to produce positron emitting isotopes. Suitable isotopes are listed in Table 1 and some reactions presented in Table 2. They can be created in a nuclear reactor or in a plasma. We shall take as examples :

- The production of  $\text{Cu}^{64}$  isotopes by thermal neutron capture of  $\text{Cu}^{63}$  in a nuclear reactor
- The creation of protons as projectiles in a  $\text{DH}_e^3$  reaction in a fusion facility.

#### $\text{Cu}^{64}$ decay

The reaction giving the desired isotope is :



$\nu$  being a neutrino.

The rate of positron production is given by [9] :

$$\frac{d}{dt} (n^+) = \gamma_{64} \cdot \overline{\sigma\Phi} \cdot V \cdot N \quad (1.15)$$

where  $\gamma_{64}$  is the  $\beta^+$  branching ratio ( $\beta^+$ /disintegration)

$\sigma$ , the cross section for  $\beta^+$  emitter production

$\Phi$ , the thermal neutron flux

$V$ , the target volume

$N$ , the target atom density.

Examination of this formula shows, as already pointed out by E. Ottewitte, that significant improvement can be obtained by increasing the thermal neutron flux and the target volume. The most serious limitation is that due to the rate at which heat can be removed.

Table 1  
Suitable positron-emitting isotopes (from E. Ottewill, ref. 9)

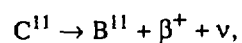
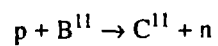
Isotope	$\tau$	$\beta^+/\text{dis}$	$\beta^+$	Production Reaction
Na <sup>22</sup>	2.6y	0.39	0.54	Mg <sup>24</sup> (d, $\alpha$ )
Al <sup>26</sup>	7.4x10 <sup>5</sup> y	0.85	1.17	Mg <sup>24</sup> (d, $\gamma$ )
Co <sup>55</sup>	18.2h	0.60	1.50, 1.03, 0.53, 0.26	Fe <sup>12</sup> (p, 2n)
V <sup>48</sup>	16.2d	0.56	0.69	Ti <sup>48</sup> (p, n)
Ni <sup>57</sup>	36h	0.50	0.85, 0.72, 0.35	Ni <sup>58</sup> (p, pn)
Sr <sup>83</sup>	33h	0.50	1.15	Sr <sup>84</sup> (p, pn)
Y <sup>86</sup>	14.6h	0.50	1.80, 1.19	Sr <sup>86</sup> (p, n)
Br <sup>76</sup>	17.2h	0.44	3.57, 1.7, 1.1, 0.8, 0.6	Se <sup>76</sup> (p, n)
Nb <sup>90</sup>	14.6h	0.40	1.51, 0.66	Zr <sup>90</sup> (p, n)
Mn <sup>52</sup>	5.7d	0.35	0.58	Cr <sup>52</sup> (p, n)
Ge <sup>69</sup>	40h	0.33	1.22, 0.61, 0.22	Ga <sup>69</sup> (p, n)
As <sup>71</sup>	62h	0.30	0.81	Ge <sup>72</sup> (p, 2n)
As <sup>72</sup>	26h	0.30	3.34, 2.50, 1.84, 0.67, 0.27	Ge <sup>72</sup> (p, n)
I <sup>124</sup>	4.5d	0.30	2.20, 1.50, 0.70	Te <sup>124</sup> (p, n)
As <sup>74</sup>	17.5d	0.29	1.53, 0.92	Ge <sup>74</sup> (p, n)
Zr <sup>89</sup>	79h	0.25	0.91	Y <sup>89</sup> (p, n)
Co <sup>56</sup>	77d	0.20	0.44, 1.50	Fe <sup>56</sup> (p, n)
Cu <sup>64</sup>	12.8h	0.19	0.65	Cu <sup>63</sup> (n, $\gamma$ )
Rb <sup>84</sup>	33d	0.17	1.63, 0.82	Sr <sup>86</sup> (d, $\alpha$ )
Co <sup>58</sup>	71d	0.15	0.47	Ni <sup>58</sup> (n, p)

### Fusion process [10]

We can consider the reaction



If the plasma is seeded with B<sup>11</sup> or C<sup>13</sup> to produce the reactions



we obtain a positron beam.

Table 2

Some (p, n) reactions producing  $\beta^+$  emission (from J. Dawson, ref. 10)

- $$D + {}^3\text{He} \rightarrow {}^4\text{He} + p \text{ (14.7 MeV)}$$
1.  $p + {}^{11}\text{B} \rightarrow {}^{11}\text{C} + n \text{ (}E_T = 2.76 \text{ MeV)}$   
 ${}^{11}\text{C} \rightarrow {}^{11}\text{B} + e^+ \text{ (}\tau_{1/2} = 20 \text{ min.)}$
  2.  $p + {}^{13}\text{C} \rightarrow {}^{13}\text{N} + n \text{ (}E_T = 3 \text{ MeV)}$   
 ${}^{13}\text{N} \rightarrow {}^{13}\text{C} + e^+ \text{ (}\tau_{1/2} = 10 \text{ min.)}$
  3.  $p + {}^{15}\text{N} \rightarrow {}^{15}\text{O} + n \text{ (}E_T = 3.53 \text{ MeV)}$   
 ${}^{15}\text{O} \rightarrow {}^{15}\text{N} + e^+ \text{ (}\tau_{1/2} = 2.03 \text{ min.)}$
  4.  $p + {}^{17}\text{O} \rightarrow {}^{17}\text{F} + n \text{ (}E_T = 3.55 \text{ MeV)}$   
 ${}^{17}\text{F} \rightarrow {}^{17}\text{O} + e^+ \text{ (}\tau_{1/2} = 66 \text{ sec.)}$
  5.  $p + {}^{18}\text{O} \rightarrow {}^{18}\text{F} + n \text{ (}E_T = 2.45 \text{ MeV)}$   
 ${}^{18}\text{F} \rightarrow {}^{18}\text{O} + e^+ \text{ (}\tau_{1/2} = 1.87 \text{ hr.)}$
  6.  $p + {}^{19}\text{F} \rightarrow {}^{19}\text{Ne} + n \text{ (}E_T = 4.03 \text{ MeV)}$   
 ${}^{19}\text{Ne} \rightarrow {}^{19}\text{F} + e^+ \text{ (}\tau_{1/2} = 18 \text{ sec.)}$
  7.  $p + {}^{26}\text{Mg} \rightarrow {}^{26}\text{Al} + n \text{ (}E_T = 5.01 \text{ MeV)}$   
 ${}^{26}\text{Al} \rightarrow {}^{26}\text{Mg} + e^+ \text{ (}\tau_{1/2} = 6.5 \text{ sec.)}$
  8.  $p + {}^{22}\text{N} \rightarrow {}^{22}\text{Na} + n$   
 ${}^{22}\text{Na} \rightarrow {}^{22}\text{Ne} + e^+ \text{ (}\tau_{1/2} = 2.6 \text{ years)}$
- $\sigma = 200 \text{ mb}$

## 2. PRESENTATION OF SOME POSITRON SOURCES

We present here some typical positron sources involving electron-generated and photon-generated electromagnetic showers, together with some details of radioactive positron sources.

### 2.1 Electron generated positron source

Positron sources used in present day accelerators are generated by a linac electron beam. The increasing positron yield with electron energy leads to the use of very energetic electron beams and linear colliders are now constructed or planned with multi-GeV incident electron beams on the converter.

We already showed that positrons produced with an electron beam are emitted with a wide energy spectrum, large angles and lateral dimensions as small as those of the impinging electron beam. As new electron sources could provide small emittance beams, lateral electron beam dimensions on the target are greatly dependent on the energy spread of the electron beam. This energy dispersion leads to an enlargement of the beam dimensions in the chromatic quadrupole channel preceding the target. Wake fields in the electron linac of the positron source give the main contribution to the energy dispersion. This induces some limitation on incident electron beam intensity. A possible scheme for an electron generated positron source is represented in Fig. 10.

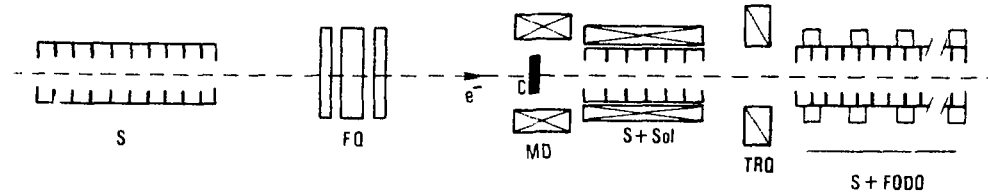


Fig. 10 Electron generated positron source

S - Accelerating section  
 FQ - Focusing triplet  
 MD - Matching device  
 Sol - Solenoid  
 TRQ - Transition optics between solenoid and FODO  
 C - Converter

## 2.2 Production of positrons using undulatory radiation

Instead of using very high energy electron beams on thick targets which require a very important amount of power, we could use photons to generate positrons by pair production in the target. The radiation of high energy electrons in the undulator is mainly concentrated in small angles relative to the electron velocity direction. This feature makes the method attractive for small positron sources. We shall consider here two kinds of undulatory radiations for creating photons :

- In a helical undulator
- By electron channeling in a crystal.

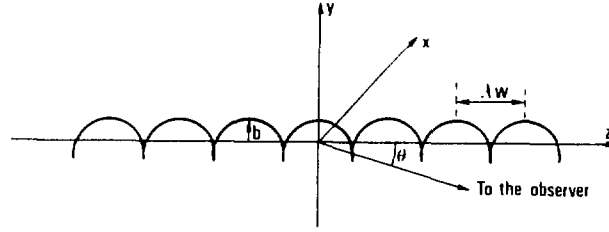
### 2.2.1. Production of positrons with photons from a helical undulator

Experiments using polarized particles are necessary in order to study the details of the interaction of high energy particles in the range of 100 GeV and above. This has led to serious interest in high intensity sources of polarized particles, especially positrons. One study has been initiated at Novosibirsk (URSS) for the VLEPP project [11] where the conversion system enables  $e^+e^-$  pairs, both polarized, to be obtained. The basic idea of the system is to use circularly polarized photons produced in a helical undulator by high energy non-polarized bunches of electrons coming from a linear accelerator. The main advantages of such a system are the circularly polarized photons which generate longitudinally polarized positrons, and the lower thermal effects in the converter due to the fact that the electron beam is not striking the target.

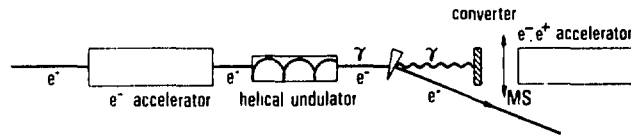
The transverse periodic helical magnetic field of constant magnitude is produced on the axis of a double-helix-wound bifilar magnet with equal and opposite currents in each helix [12]. The orbit of the high energy electron in the helical magnetic field  $B$  is a helix having the same period,  $\lambda_w$ , as the field. The radius is given by :

$$b = \left( \frac{\lambda_w}{2\pi\rho} \right)^2 \rho \left[ 1 - \left( \frac{\lambda_w}{2\pi\rho} \right)^2 \right]^{1/2} \quad (2.1)$$

with  $\rho = \gamma\beta mc^2/eB$ , and where  $\beta$  and  $\gamma$  are the normalized velocity and energy.



a) Physical parameters used in the text



b) Lay out of a positron source using a magnetic undulator

Fig. 11 Generation of positrons with photons from a helical undulator

Synchrotron radiation is emitted in a conical angle of  $\theta \approx 1/\gamma$  around the electron direction of motion (Fig. 11a). If the electron energy is very high and the number,  $N$ , of periods in the undulator very large, we have for paraxial photons a spectrum consisting of a narrow-peak at :

$$\lambda = \frac{\lambda_w}{2\gamma^2} (1 + K^2) \quad (2.2)$$

where  $\gamma$  is the relative electron energy,

and

$$K = \frac{\lambda_w e B}{2\pi mc} \quad (2.3)$$

The energy bandwidth is about  $1/N$  and obviously depends on the angular divergence of the electron beam which must be restricted to :

$$\theta_{\max} = [\gamma\sqrt{N}]^{-1}. \quad (2.4)$$

For  $K = 1$ , we get for the peak energy of the photons :

$$E_{\gamma} = \frac{2\pi \hbar c}{\lambda_w} \gamma^2.$$

For any  $K$  value, we get :

$$E_{\gamma} = \frac{4\pi \hbar c \gamma^2}{\lambda_w (1 + K^2)}, \quad (2.5)$$

the rate of energy loss by radiation being [13]

$$P_{\gamma} = \frac{2}{3} \frac{r_e c}{(mc^2)^3} E^2 F_{\perp}^2 \quad (2.6)$$

where  $E$  is the electron energy and  $F_{\perp} = e c B$ .

We get for the total radiated energy of an electron :

$$\Delta w = \frac{8}{3} \pi^2 r_e mc^2 \frac{\gamma^2 K^2 N}{\lambda_w} \quad (2.7)$$

So, the corresponding number of photons is [14] :

$$N_{\gamma} = \frac{2}{3} \pi r_e \frac{mc^2}{\hbar c} K^2 (1 + K^2) N$$

or

$$N_{\gamma} = \frac{2}{3} \pi \alpha K^2 (1 + K^2) N \quad (2.8)$$

where  $\alpha = 1/137$ .

Ex : For a 100m undulator with a periodic length  $\lambda_w = 1$ cm, an electron of 100 GeV energy generates 250 photons of 5.3 MeV.

The positron yield is given by :

$$\eta^+ = N_{\gamma} n^+ \quad (2.9)$$

where  $n^+$  is the number of positrons accepted by a given system expressed by :

$$n^+ = n_0 \iiint f_E(E) f_r(r,E) f_{\theta}(\theta,E) dE dr 2\pi \sin\theta d\theta \quad (2.10)$$

where  $n_0$  is the total number of positrons generated by an incident photon on the target,  $f_E$ ,  $f_{\theta}$  and  $f_r$  being given by EGS simulations as in the electron generating case. The limits of integration are given by the acceptance parameters of the matching system. A scheme of the positron production using this method is given in Fig. 11b.

Ex : For a 0.2 Xo thick tungsten target, 5.3 MeV photons generate positrons with a yield of  $8.10^{-3} e^+/\gamma$ . We get then  $2 e^+/e^-$  as total yield. Acceptance limitations significantly lower this value. To get higher  $e^+/e^-$  yield values one has to increase the electron beam energy and/or increase the undulator length.

### 2.2.2 *Positron source generated by photons from channeled particles*

Instead of generating high energy photons by synchrotron radiation in a wiggler, we can make use of the atomic potentials in a crystal. Photon emission processes or pair creation in the crystal generated by incident particles ( $e^-$  or  $\gamma$ ) propagating in the vicinity of the crystal axis, present different features than those of the classical interaction of incident particles with an amorphous medium, provided the angle of incidence of these particles is smaller than a critical angle :

$$\theta_c = \sqrt{\frac{2V_0}{E_0}} \quad (2.11)$$

where  $E_0$  is the particle energy,

$V_0$  is the potential given by the atomic rows.

The particles undergo collective interaction with some subset of regularly situated atoms in the crystal lattice (Fig. 12).

Incident particle trajectories in the crystal are very similar to those in a magnetic wiggler with a periodicity several times the atomic separation distance. This atomic wiggler presents high levels of photon production which can be used to generate positrons via pair creation in an amorphous target. However, pair creation in the crystal demands very high energy levels (more than 50 GeV) to exceed the classical Bethe - Heitler cross sections in the amorphous medium. Nevertheless, this method of producing positrons could be interesting provided that thermic and radiation effects using high intensity incident beams do not affect the crystal structure. The feasibility of such a method is under study [15].

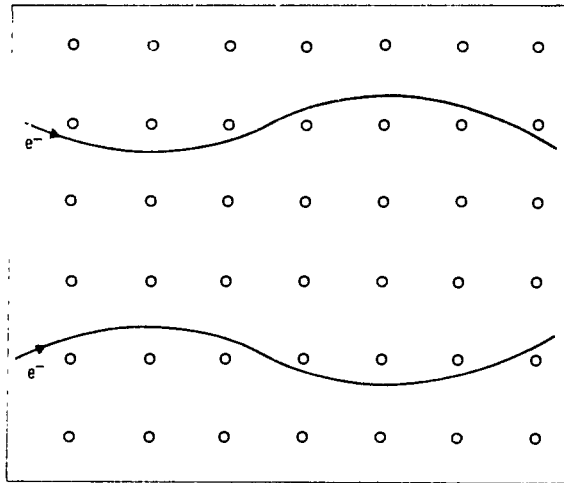


Fig. 12 Electron channeling in a crystal. This drawing is considerably exaggerated. Oscillations of channeled particles occur with wavelengths of thousands of lattice spacings.

### 2.3 Radioactive sources

We shall take as an example of a radioactive source that designed for the BNL experiment [9] which uses the  $\text{Cu}^{64}$  decay. In this case the rate of positron production (Eq. (1.15)) is :

$$\frac{d}{dt} (n^+) = \underbrace{0.19}_{\beta^+} \times \underbrace{3.6 \times 10^{-24}}_{\overline{\sigma_{63\phi}}} \times \underbrace{\frac{1}{16}}_V \times \underbrace{0.075 \times 10^{24}}_N \times \underbrace{0.8}_{\text{after some irradiation period}}$$

i.e., 
$$\frac{d}{dt} (n^+) = 2.1 \times 10^{12} \text{ e}^+/\text{s}.$$

Higher  $e^+$  fluxes have been obtained by test reactors as INEL/ATR (Idaho National Engineering Laboratory -US Navy) with more than  $10^{17} \text{ e}^+/\text{s}$ . These reactors require large irradiation volumes to perform multi-magnitude increase in positron production. Thus, the INEL/ATR has nine large channels presenting a total irradiation volume of  $2.6 \times 10^4 \text{ cm}^3$  ; such a facility allows more than a factor of 5 in magnitude improvement of the positron production.

As mentioned before,  $e^+$  rate improvement using larger source volumes poses two difficult problems :

- How to transform from a large, voluminous positron source into a compact beam
- Increasing the volume may lead to self absorption, so a limitation on thickness exists.

### 3. POSITRON COLLECTION : THE MATCHING SYSTEM

The characteristic emittance of the positron source at the converter – large angles, small lateral dimensions – has to be transformed into small angles, large lateral dimensions, so as to fit with the accelerator acceptance. The choice of the matching device is therefore dependent on :

- The expected positron yield
- The allowed energy dispersion.

Two kinds of matching devices are now mainly used on positron accelerators :

- Narrow band systems such as the quarter wave transformer
- Large band systems such as the adiabatic device.

Other kinds of matching devices such as the lithium and plasma lens may also be used.

#### 3.1 Matching devices using a solenoidal magnetic field [4,16]

##### 3.1.1 The solenoidal magnetic field

Due to the cylindrical symmetry of the solenoid about the z axis, the only non-zero component of the potential vector  $\vec{A}$  in cylindrical coordinates (r,  $\phi$ , z) is :

$$A_{\phi} = \frac{r}{2} B(z) - \frac{1}{16} r^3 \frac{d^2 B}{dz^2}. \quad (3.1)$$

The Lagrangian,

$$L = -m_0 c^2 \sqrt{1 - v^2/c^2} - e (\mathbf{V} - \vec{A} \cdot \vec{v})$$

may be expressed in these coordinates as :

$$L = -m_0 c^2 \sqrt{1 - \frac{(\dot{r}^2 + r^2 \dot{\phi}^2 + \dot{z}^2)}{c^2}} - e \left( \dot{z} - r^2 \dot{\phi} \frac{B}{2} \right). \quad (3.2)$$

Conjugate variables (q, p) are defined by :

$$p = \frac{\partial L}{\partial \dot{q}}. \quad (3.3)$$

We can therefore observe that the absence of  $\phi$  in the expression of L gives

$$p_{\phi} = \text{constant}$$

which expresses the invariance of the angular momentum.

The transport matrix of the solenoid can be represented in the following way. The Lagrange equation :

$$\frac{d}{dt} \cdot \frac{\partial L}{\partial \dot{q}_j} - \frac{\partial L}{\partial q_j} = 0 \quad (3.4)$$

gives with cartesian coordinates :

$$\frac{d}{dz} \left( P \frac{dx}{dz} - \frac{eB}{2} y \right) = \frac{eB}{2} \frac{dy}{dz} \quad \text{and} \quad \frac{d}{dz} \left( P \frac{dy}{dz} + \frac{eB}{2} x \right) = -\frac{eB}{2} \frac{dx}{dz} \quad (3.5)$$

where P represents the scalar momentum

A convenient way to handle the particle dynamics in a solenoidal magnetic field is to transform these coordinates into rotating ones  $(\xi, \eta)$  with a rotation angle given by the Larmor angle

$$\chi = \int_0^z \frac{eB}{2P} dz. \quad (3.6)$$

Such a transformation is represented by :

$$\begin{pmatrix} \xi \\ p_\xi \\ \eta \\ p_\eta \end{pmatrix} = \begin{pmatrix} \cos \chi & 0 & -\sin \chi & 0 \\ 0 & \cos \chi & 0 & -\sin \chi \\ \sin \chi & 0 & \cos \chi & 0 \\ 0 & \sin \chi & 0 & \cos \chi \end{pmatrix} \begin{pmatrix} x \\ p_x \\ y \\ p_y \end{pmatrix}. \quad (3.7)$$

The equations of motion are then :

$$p'_\xi = \frac{d}{dz} (P\xi') = -\left(\frac{eB}{2}\right)^2 \cdot \frac{\xi}{P} \quad (3.8)$$

$$p'_\eta = \frac{d}{dz} (P\eta') = -\left(\frac{eB}{2}\right)^2 \cdot \frac{\eta}{P}.$$

Motions for  $\xi$  and  $\eta$  are decoupled and can be handled separately. The equations (3.8) may be written :

$$\xi'' + \frac{P'}{P} \xi' + \left(\frac{eB}{2P}\right)^2 \xi = 0 \quad (3.9)$$

$$\eta'' + \frac{P'}{P} \eta' + \left(\frac{eB}{2P}\right)^2 \eta = 0.$$

For a constant field B, and in the absence of an accelerating field, these equations are those of a classical harmonic oscillator of constant frequency  $\frac{eB}{2P}$ . The transformation matrix is then, in the  $(\xi, p_\xi)$  plane for example,

$$\begin{pmatrix} \xi \\ p_\xi \end{pmatrix} = \begin{pmatrix} \cos \chi & \frac{2}{eB} \sin \chi \\ -\frac{eB}{2} \sin \chi & \cos \chi \end{pmatrix} \begin{pmatrix} \xi_0 \\ p_{\xi 0} \end{pmatrix} \quad (3.10)$$

We can associate with the variables  $(\xi, p_\xi)$  and  $(\eta, p_\eta)$ , the Hamiltonians :

$$H_1 = \frac{eBc}{4P} \left[ \frac{eB}{2} \xi^2 + \frac{2}{eB} p_\xi^2 \right] \quad (3.11)$$

$$H_2 = \frac{eBc}{4P} \left[ \frac{eB}{2} \eta^2 + \frac{2}{eB} p_\eta^2 \right].$$

If we define a frequency  $\omega = \frac{eBc}{4\pi P}$ , the quantity :

$$\frac{H}{\omega} = \pi \left[ \frac{eB}{2} \xi^2 + \frac{2}{eB} p_\xi^2 \right] \quad (3.12)$$

is an adiabatic invariant of the motion. So, we can write :

$$\left(\frac{eB}{2}\right)^2 (\xi^2 + \eta^2) + (p_\xi^2 + p_\eta^2) = \text{constant.}$$

Coming back to the variables  $[x, p_x; y, p_y]$ , we may write :

$$\left(\frac{eB}{2}\right)^2 (x^2 + y^2) + p_x^2 + p_y^2 = \text{constant.} \quad (3.13)$$

This relation holds everywhere in the solenoid. It represents the equation of an hyperellipsoid in the phase space  $[x, p_x; y, p_y]$ . The volume comprised in this hyperellipsoid is constant [Liouville Theorem].

### 3.1.2 Narrow band system : The quarter wave transformer (QWT)

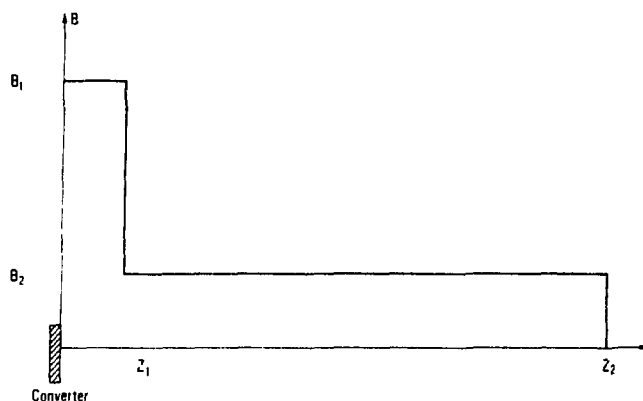


Fig. 13 Field profile of the quarter wave transformer

This system is widely used in positron accelerators. It is made from a short lens with a high magnetic field and a long solenoidal magnetic field extending over several accelerating sections [17]. Such a field profile is represented in Fig. 13. The most recent versions of this device use a short pulsed lens with a high magnetic field just after the converter in the vacuum chamber (DESY [18], Frascati [19], LEP [20], KEK [21]).

We can associate with the transport matrix of the system – which is symplectic – a quadratic form :

$$\begin{aligned} XX^* + \left(\frac{2}{eB_2}\right)^2 P_X P_X^* &= \left( \cos^2 \chi_1 + \left(\frac{B_1}{B_2}\right)^2 \sin^2 \chi_1 \right) X_0 X_0^* + \left[ \left(\frac{2}{eB_1}\right)^2 \sin^2 \chi_1 + \left(\frac{2}{eB_2}\right)^2 \cos^2 \chi_1 \right] P_{X0} P_{X0}^* \\ &+ \frac{2}{eB_1} \sin \chi_1 \cos \chi_1 \left[ 1 - \left(\frac{B_1}{B_2}\right)^2 \right] (X_0^* P_{X0} + X_0 P_{X0}^*) \end{aligned} \quad (3.14)$$

where  $X = x + iy$ ,  $P_X = p_x + ip_y$

$X^*$  and  $P_X^*$  are the conjugate values,

$\chi_1$  represents the Larmor angle followed by the particle in the first lens.

We may observe that :

$$\left(\frac{eB_2}{2}\right)^2 XX^* + P_X P_X^* = \left(\frac{eB_2}{2}\right)^2 (x^2 + y^2) + (p_x^2 + p_y^2) = C, \quad (3.15)$$

C being a constant.

A positron emitted on the converter with a scalar momentum  $P_0$  and phase space coordinates  $X_0$  and  $P_{X_0}$  can be transmitted at the end of the (long) solenoid only if :

$$XX^* \leq a^2 \quad (3.16)$$

where  $a$  represents the iris radius of the accelerating cavities. This condition implies :

$$C - \left(\frac{2}{e B_2}\right)^2 P_X P_X^* \leq a^2$$

or in cylindrical coordinates,

$$C - \left(\frac{2}{e B_2}\right)^2 \left[ p_r^2 + \frac{p_\phi^2}{r^2} \right] \leq a^2$$

which gives the value of

$$C = a^2 + \left(\frac{2}{e B_2}\right)^2 \cdot \frac{p_\phi^2}{a^2}. \quad (3.17)$$

The set of points in the phase space which satisfy the condition (3.16) constitute the acceptance volume of the system.

We may write, using the cylindrical coordinates  $(r, \phi, p_r, p_\phi)$ , and for  $\chi_1 = \frac{\pi}{2}$ , the quadratic form corresponding to the acceptance figure :

$$\left(\frac{B_1}{B_2}\right)^2 \cdot \left(\frac{r_0}{a}\right)^2 + \left(\frac{p_{r_0}}{e B_1 a}\right)^2 + \left(\frac{p_{\phi_0}}{e B_1 a^2}\right)^2 \left[ \frac{1}{\left(\frac{r_0}{a}\right)^2} - \frac{1}{\left(\frac{B_2}{B_1}\right)^2} \right] = 1. \quad (3.18)$$

We may define [22] :

$$\frac{r_0}{a} = \rho, \quad \frac{p_{r_0}}{e B_1 a} = \zeta, \quad \frac{p_{\phi_0}}{e B_1 a^2} = \Phi$$

Equation (3.18) then becomes :

$$\left(\frac{B_1}{B_2}\right)^2 \rho^2 + \zeta^2 + \Phi^2 \left[ \frac{1 - \left(\frac{B_1}{B_2}\right)^2 \rho^2}{\rho^2} \right] = 1. \quad (3.19)$$

Integration of the volume comprised in the hyperellipsoid gives :

$$\mathcal{V} = 2\pi^2 \left(\frac{e B_1 a^2}{2}\right)^2 \int_0^{\rho_{\max}} \sqrt{1 - \left(\frac{B_1}{B_2}\right)^2 \rho^2} \rho d\rho. \quad (3.20)$$

However, integration is feasible only if :

$$\rho = \frac{r_0}{a} \leq \frac{B_2}{B_1}. \quad (3.21)$$

This condition defines the radial acceptance of the system. Then, we obtain :

$$\mathcal{V} = \frac{2\pi}{3} \left( \frac{e B_2 a^2}{2} \right)^2. \quad (3.22)$$

Therefore, the acceptance volume expression of the quarter wave transformer calculated for  $\chi_1 = \frac{\pi}{2}$ , i.e for particles with a half helical period in the short lens, has a close dependence on the radius of the iris as well as on the strength of the solenoid magnetic field.

The total acceptance of the system is obtained if we evaluate the contributions from the particles emitted at the converter in the whole energy spectrum i.e for any  $\chi_1$ . In this case, the hyperellipsoid equation is given by [4]:

$$\begin{aligned} & \left[ \cos^2 \chi_1 + \left( \frac{B_1}{B_2} \right)^2 \sin^2 \chi_1 \right] r_0^2 + \left[ \left( \frac{2}{eB_1} \right)^2 \sin^2 \chi_1 + \left( \frac{2}{eB_2} \right)^2 \cos^2 \chi_1 \right] \left( p_{r_0}^2 + \frac{p_{\phi 0}^2}{r_0^2} \right) \\ & + \frac{4}{eB_1} \sin \chi_1 \cos \chi_1 \left[ 1 - \left( \frac{B_1}{B_2} \right)^2 \right] r_0 p_{r_0} = a^2 + \left( \frac{2}{eB_2} \right)^2 \frac{p_{\phi 0}^2}{a^2}. \end{aligned} \quad (3.23)$$

Integration of the volume comprised in the acceptance hyperellipsoid gives :

$$\mathcal{V}(\chi_1) = \frac{2\pi}{3} \left( \frac{eB_2 a^2}{2} \right)^2 \left[ 1 - \left( 1 - \frac{1}{\sin^2 \chi_1 + \left( \frac{B_1}{B_2} \right)^2 \cos^2 \chi_1} \right)^{3/2} \right]. \quad (3.24)$$

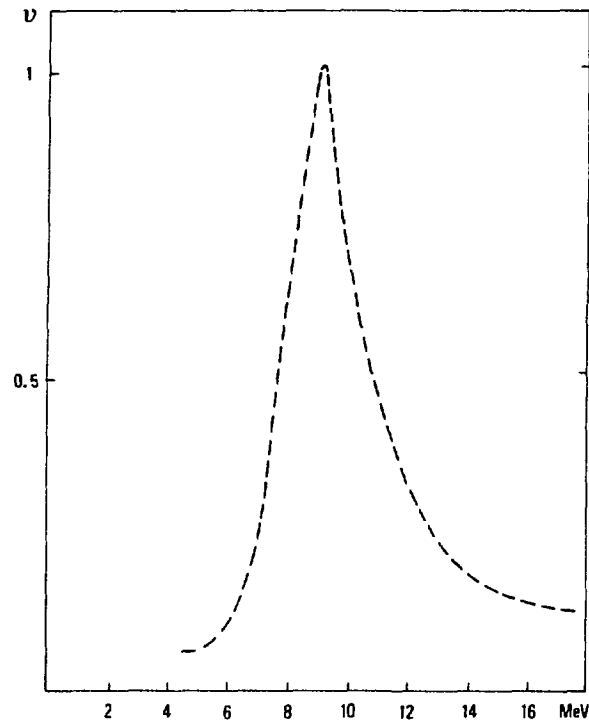


Fig. 14 Acceptance volume for a QWT

Figure 14 represents this acceptance volume for a quarter wave transformer defined by :

$$B_1 = 20 \text{ kgauss}$$

$$B_2 = 4 \text{ kgauss}$$

$$L = 4.7 \text{ cm (short lens length).}$$

The angular acceptance in each plane may be calculated by observing that the maximum  $p_x$  or  $p_y$  value at the converter plane is  $\left(\frac{e B_1}{2} a\right)$ . Since :

$$p_x = P_x' + e A_x$$

and

$$x_0 (p_x \text{ max}) = 0$$

and

$$y_0 (p_x \text{ max}) = r_0 = \frac{B_2}{B_1} a$$

we get :

$$\theta_{\text{max}} = x'_{\text{max}} = \frac{e B_1 a}{2P} \left[ 1 + \frac{B_2}{B_1} \right]. \quad (3.25)$$

A convenient representation of the phase space is given by the intersection of the hyperellipsoid with the plane ( $y_0 = 0$  ;  $p_{y0} = 0$ ) as shown in Fig. 15.

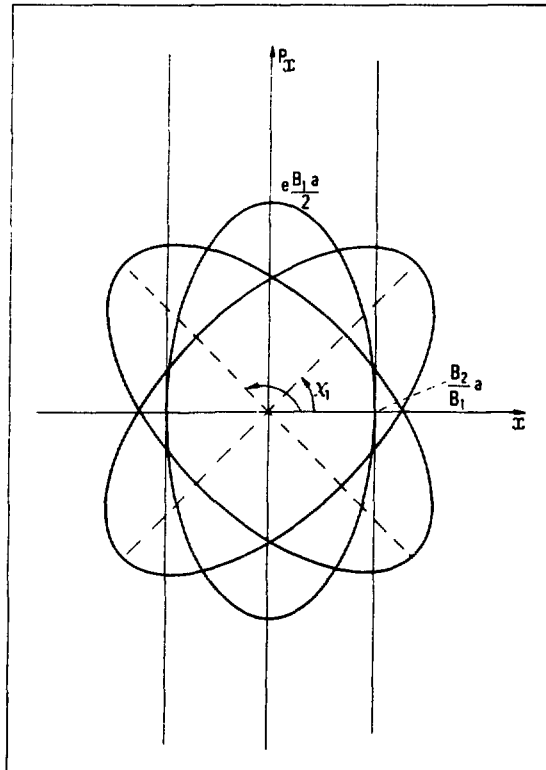


Fig. 15 Intersection of the hyperellipsoid with the plane ( $y_0 = 0$  ;  $p_{y0} = 0$ ) for the QWT

### 3.1.3 Large band system : The adiabatic device (AD)

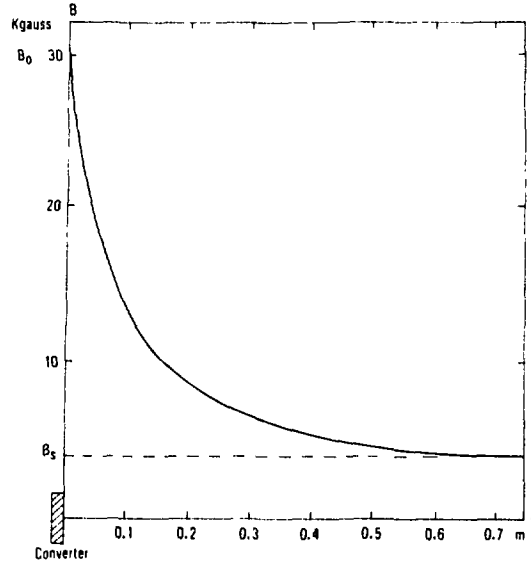


Fig. 16 Field profile of the adiabatic device

This system used at SLAC [23] and Orsay [24] is made of a slowly varying magnetic field lens followed by a long solenoidal magnetic field extending over some accelerating sections. Between the maximum ( $B_0$ ) and the minimum ( $B_s$ ) values, the magnetic field adiabatically tapers (see Fig. 16) so as to conserve the adiabatic invariant :

$$\oint \sum_i p_i dq_i = \frac{\pi p_{\perp}^2}{eB} \quad (3.26)$$

where  $(q_i, p_i)$  are the conjugate variables  
 $p_{\perp}$  the transverse momentum and,  
 $B$  the field strength.

If the magnetic field changes slowly, so does the period of the motion and the adiabatic invariant  $J = \frac{A}{\pi}$ . The parameter of smallness  $\epsilon$  of this variation must be very weak. So :

$$\epsilon = \frac{P}{eB^2} \cdot \frac{dB}{dz} \ll 1. \quad (3.27)$$

#### Transport matrix

With a slowly varying magnetic field, Eq (3.9) may be integrated using the WKBJ Method [25] and under the assumption (3.27), we obtain the expression of the transport matrix in the rotating frame :

$$\begin{pmatrix} \xi \\ p_{\xi} \end{pmatrix} \begin{pmatrix} \left[ \frac{B_0}{B} \right]^{1/2} \cos\phi & \frac{2}{e[B_0 B]^{1/2}} \sin\phi \\ -\frac{e[B_0 B]^{1/2}}{2} \sin\phi & \left[ \frac{B}{B_0} \right]^{1/2} \cos\phi \end{pmatrix} \begin{pmatrix} \xi_0 \\ p_{\xi_0} \end{pmatrix}. \quad (3.28)$$

The adiabatic magnetic field varies along  $z$  following :

$$B(z) = \frac{B_0}{1 + \mu z} \quad (3.29)$$

where  $\mu = \frac{\epsilon B_0}{P_0}$

$\epsilon$ , the parameter of smallness and

$P_0$  a particular (central value) of the scalar momentum for the emitted positron. As before, a quadratic form may be worked out using the transport matrix (symplectic) of the whole system.

#### Acceptance considerations

The quadratic form is given by :

$$XX^* + \left(\frac{2}{eB_s}\right)^2 P_X P_X^* = \left[\frac{B_0}{B_s}\right] X_0 X_0^* + \frac{4}{e^2 [B_0 B_s]} P_{X_0} P_{X_0}^* = \text{constant} . \quad (3.30)$$

Applying the condition (3.16), we get for the acceptance hyperellipsoid :

$$\left[\frac{B_0}{B_s}\right] \left(\frac{r_0}{a}\right)^2 + \left(\frac{P_{r_0}}{e\sqrt{B_0 B_s} a}\right)^2 + \left(\frac{P_{\phi_0}}{e B_s a^2}\right)^2 \left[\frac{B_s}{B_0} \cdot \frac{1}{\left(\frac{r_0}{a}\right)^2} - 1\right] = 1. \quad (3.31)$$

Integration of the phase-space volume comprised in the hyperellipsoid gives the acceptance volume :

$$\mathcal{V} = 2\pi^2 \frac{B_0}{B_s} \left(\frac{e B_s a^2}{2}\right)^2 \int_0^{\rho_{\max}} \sqrt{1 - \frac{B_0}{B_s} \rho^2} \rho d\rho . \quad (3.32)$$

Under the assumption :

$$\rho = \frac{r_0}{a} \leq \sqrt{\frac{B_s}{B_0}} \quad (3.33)$$

which constitutes the radial acceptance condition for the adiabatic system, we get :

$$\mathcal{V} = \frac{2\pi^2}{3} \left(\frac{e B_s a^2}{2}\right)^2 . \quad (3.34)$$

This acceptance volume is calculated regardless of the positron energies.

The positron energy does not appear in the hyperellipsoid equation as it did for the quarter wave transformer. The adiabatic system presents a very large energy acceptance. However, all these results have been calculated with the condition (3.27) fulfilled whereas for a given field law, not all the particles obey this condition. In particular, the high energy positrons make the parameter  $\epsilon$  too big and, hence, a high energy limitation exists.

The angular acceptance may be calculated as done previously for the QWT. We get :

$$\theta_{\max} = \frac{e\sqrt{B_0 B_s}}{P} . \quad (3.35)$$

As before, we show in Fig. 17 the intersection of the phase-space volume with the plane ( $y_0 = 0$  ;  $p_{y_0} = 0$ ).

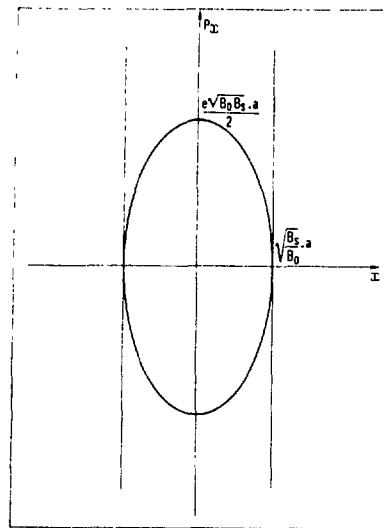


Fig 17 Intersection of the hyperellipsoid with the plane ( $y_0 = 0$  ;  $p_{y_0} = 0$ )  
for the adiabatic matching system

It is worth remarking that a comparison between the two systems may be made assuming  $B_1 = B_0$  and  $B_2 = B_5$ . We then notice that :

- Radial acceptance is larger in the adiabatic case
- Angular acceptance is larger in the QWT case
- Energy acceptance is much larger in the adiabatic case.

### 3.2 Other magnetic devices

Strong focusing devices such as lithium and plasma lenses are already in use or under study for antiproton as well as positron collection.

#### Lithium lens

Instead of using a longitudinal magnetic field, one can use an azimuthal field created by a current circulating longitudinally as the positron velocity [26]. Such a lens is made of liquid lithium in a tube only a few cm long. It has been used at Novosibirsk, FERMILAB and CERN, and is optimised to focus low energy particles (some MeV) while presenting a fairly good acceptance angle ( $\alpha > 0.5$  rad). The multiple scattering angle is about 50 mrad at 20 MeV and very high intensity currents produce magnetic fields of several Tesla. Moreover, due to the azimuthal nature of the field, positrons are focused while electrons are lost, which greatly simplifies beam control and optimisation.

#### Plasma lens

If we look at a non-absorbing medium with an azimuthal magnetic field created by a longitudinal current, the plasma lens could give an interesting opportunity with high magnetic fields. In the plasma lens based on the Z-pinch effect, the conductor is a column of ionized gas –hydrogen for example–. A high intensity pulsed current created with an appropriate discharge circuit and flowing through the ionized gas produces an imploding plasma column. The positrons moving through the plasma when the "pinch" is reached, are strongly focused by the azimuthal magnetic field. Such a device has been studied in many laboratories and especially at CERN for the antiproton source of the ACOL project [27].

### 3.3 Phase slippage in the matching system

Phase slippage makes some contribution to positron beam energy spread. At some distance from the converter, we can write for the positron beam energy dispersion :

$$\Delta E^+ = [ \Delta E_s^2 + \Delta E_\phi^2 ]^{1/2}$$

where  $\Delta E_s$  is the energy dispersion at the converter i.e., the accepted energy spread.  $\Delta E_\phi$  is the contribution of phase slippage to energy dispersion and arises from the difference in velocities of the accepted positrons, and from the path-length differences of trajectories in the magnetic fields.

#### Phase slippage due to difference in velocities

The phase slippage is given by :

$$\Delta\phi_v = \frac{\pi}{\lambda_{RF}} \cdot \int_0^L \left( \frac{1}{\gamma^2} - \frac{1}{\Gamma^2} \right) dz \quad (3.36)$$

where  $\lambda_{RF}$  is the RF wavelength ;

$\Gamma$  is the reference particle energy in units of  $m_0c^2$ .

#### Phase slippage due to path-length differences

The path-length differences occur in the matching device and constant field solenoid. So, we can write for the QWT [28] :

$$\Delta\phi_\ell = \frac{2\pi}{\lambda_{RF}} \cdot \frac{a^2}{\gamma_c \lambda_2} \left[ \frac{\pi}{4} \cdot \frac{\lambda_2}{\Lambda_1} \left( 1 + \frac{\lambda_2^2}{\Lambda_1^2} \right) + \frac{2}{\alpha \lambda_2} \right] \quad (3.37)$$

where

$$\lambda_2 = \frac{2 m_0 c}{e B_2}, \quad \Lambda_1 = \frac{2 m_0 c}{e B_1}$$

$\gamma_c$  is the central energy in units of  $m_0c^2$  (energy corresponding to half helical period followed in the short lens)

$\alpha$  is the accelerating gradient.

For the adiabatic device, we can also write :

$$\Delta\phi_\ell = \frac{2\pi}{\lambda_{RF}} \cdot \frac{a^2}{\gamma_c \lambda_s} \left[ \frac{1}{\epsilon} \text{Log} \frac{\lambda_s}{\Lambda_0} + \frac{2}{\alpha \lambda_s} \right]$$

where  $\epsilon$  is the parameter of smallness.

$$\lambda_s = \frac{2 m_0 c}{e B_s}, \quad \Lambda_0 = \frac{2 m_0 c}{e B_0}$$

The energy dispersion due to phase slippage is roughly given by :  $\frac{\Delta E}{E} \# \frac{1}{8} (\Delta\phi)^2$ .

#### 4. EMITTANCE TRANSFORMATION AND PRESERVATION

The solenoidal magnet system which is used after the matching system requires high power. A quadrupole focusing system is generally inserted some distance after the solenoid, typically when positrons have an energy of about 100 MeV. The transition between solenoidal and quadrupole focusing is made as soon as the spacing between the quadrupoles allows this. The quadrupoles are thus put on the accelerating sections with a FODO sequence. A matching device is generally inserted between the solenoid and the quadrupole systems to transform the axisymmetric beam coming from the solenoid into the well known elliptical shape of the FODO system. The positron beam transverse emittance is quite large, 2 to 5 MeV/c mm or,

$$\epsilon_n = 4.10^{-3} \text{ to } 10^{-2} \text{ mm mrad.}$$

This emittance has to be reduced before the interaction point in damping rings (DR) producing synchrotron radiation. Damping and excitation due to quantized emission of photons provide an equilibrium beam size which is smaller than that entering the DR.

Since the required positron bunch length is usually shorter than that delivered by the DR, bunch length compression, has to be applied. This is done in a two-stage process :

- Acceleration of the bunch in a RF cavity, the phase of the bunch centre is at  $0^\circ$  so as to accelerate the particles ahead of this point and decelerate those behind
- Non isochronous transport of the bunch, the higher energy particles travelling on a longer path than those of lower energy.

As a result, all the positrons arrive at the linac entrance at almost the same time so that the bunch length is shortened while the energy spread is increased.

Geometrical misalignments in a linac cause perturbations of the beam trajectory. Since the positron beam emittance before damping is relatively large, accurate steering to avoid beam losses in the accelerating sections is required. Trajectory perturbations can be caused by quadrupole misalignments (displacements and rotation of the quadrupole axis), accelerating - section misalignments and gradient errors. Analytical evaluations have shown that the lateral quadrupole displacement is the most critical misalignment while tilt around one of their transverse axes is the effect next in importance. Trajectory control using beam position monitors associated with steering dipoles allows the beam lateral displacements to be minimised and hence prevents significant wake field perturbations for high intensity positron beams [29].

#### 5. COMPARISON BETWEEN POSITRON SOURCES

A comparison between positron sources – existing or starting – is presented in table 3. The two parameters associated with the incident electron beam, peak intensity  $I^-$  or number of electrons per bunch  $N^-$  and energy  $E^-$ , are represented by their values at the converter location. Target material and matching device are also indicated. The two magnetic field values represent  $(B_1, B_2)$  and  $(B_0, B_S)$  for the quarter wave transformer and the adiabatic device respectively. Positron yield normalized to 1 GeV incident electron beam is reported for three corresponding measurements :

- As close as possible from the target (total yield)
- At the linac output
- In the beam switchyard ; slit width is indicated in % of the final energy.

Emittance measurements are also reported.

Some remarks can be inferred from this table :

- 1) Normalized positron yield values are almost between 2 and  $4 \times 10^{-2} e^+/e^-$  for total accelerated particles.
- 2) The useful yield – in a given energy slit – is roughly half of the Linac output yield for a 1 % energy bandwidth. For the SLC this useful yield is obviously very close to the linac output yield due to the high final energy.
- 3) Undamped positron emittances scale from  $\pi$  to more than  $4\pi$  mm mrad for a 1 GeV positron beam. Discrepancies are quite important between the measurements. Different acceptance features of the positron linacs do not completely explain that. The very small emittance of the SLC positron beam – two orders of magnitude lower than the others – is obviously due to the damping ring.

Table 3

Laboratories	e <sup>-</sup>		e <sup>+</sup> source		e <sup>+</sup> /e <sup>-</sup> GeV <sup>-1</sup>			Emittance mm. mrad
	I <sup>-</sup> A or (N <sup>-</sup> )	E <sup>-</sup> GeV	Target	Matching	Total yield	Linac output	Beam switchyard	
LEP (LIL)	2.5	0.2	W	QWT 18 - 3 kgauss		$2.5 \times 10^{-2}$	$1.5 \times 10^{-2}$ ( $\pm 1\%$ )	$6\pi$ (500 MeV)
DESY	1.4	0.28	W	QWT 20 - 3 kgauss		$4 \times 10^{-2}$	$2.4 \times 10^{-2}$ ( $\pm 0.5\%$ )	$13\pi$ (360 MeV)
A.L.S. (Saclay)	0.006	0.1	W - Re	QWT 12.5 - 3 kgauss		$2 \times 10^{-2}$	$10^{-2}$ ( $\pm 0.5\%$ )	$3\pi$ (350 MeV)
LAL (Orsay)	0.8	1	W	AD 12.5 - 1.8 kgauss	$3 \times 10^{-2}$	$2 \times 10^{-2}$	$10^{-2}$ ( $\pm 0.5\%$ )	$2\pi$ (1 GeV)
SLC	$(2 \times 10^{10})$	33	W - 26 Re	AD 50 - 5 kgauss	$7 \times 10^{-2}$	$2.6 \times 10^{-2}$	$2.6 \times 10^{-2}$ ( $\pm 0.2\%$ )	$3\pi \times 10^{-4}$ (50 GeV)

## 6. SUMMARY AND CONCLUSIONS

Quantitative results on positron production using shower codes are available and allow precise determination of the expected number of positrons. These results can be compared to the measurements carried out on existing positron sources. Reliable matching systems working in many laboratories give the possibility of choosing the device which is the most adapted to the problem.

If we consider a positron source devoted to a linear collider, we notice that the required maximization of the luminosity induces some stringent conditions on positron beams. The requirements concern intense bunches for positrons as for electrons, very small emittances and a high repetition rate. The small emittance constitutes an attainable goal as shown by the SLC experience using damping rings. However, the large number of particles per bunch – from  $10^{10}$  to  $10^{12}$  – and the high repetition frequency seem somewhat difficult to handle if one requires a high number of impinging electrons on the positron target to produce the required bunch population.

Since beam intensity is limited by wake-field effects, one cannot increase the intensities of the positron beam by simply increasing the electron beam intensity well above the positron intensity needed. So we are led to a

yield of  $1 e^+/e^-$ , at least concerning the accepted positrons. Moreover, thermic and radiation problems in the target limit the incident electron power. If the interest associated with high energy electron beams is clearly demonstrated, one has to consider the effects of a large number of particles impinging on a small area of the target. Rotating targets could be a solution.

Semi-classical methods using photons instead of electrons on amorphous targets may offer attractive alternatives for future  $e^+$  sources while radioactive sources, though offering the possibility of large numbers of  $e^+$  as in the test reactors, present too many difficulties.

Much work remains to be done !

\* \* \*

### REFERENCES

- [ 1] B. Rossi, High Energy Particles, Prentice Hall, Ed. (1956)
- [ 2] W.R. Nelson, R.L. Ford, The EGS code system, SLAC 210 (1978)
- [ 3] A. Crawford, M. Messel, Electron - photon shower distribution function tables for lead, copper and air absorbers, Pergamon Press, Oxford (1970)
- [ 4] R. Chehab, Etude de la production et du confinement d'un faisceau de positrons. Application à l'Accélérateur Linéaire d'Orsay, RI/75-4 (Avril 75)
- [ 5] M. De Staebler, More calculations for positron target test in ESA  
Internal memo CN-24 (Avril 1980)
- [ 6] S. Ecklund, Positrons for linear colliders, SLAC Pub 4484 (Nov. 87)
- [ 7] P. Sievers, M. Höfert, Radiological problems at high energy, high intensity electron-positron converters - CLIC note 71 (July 1988)
- [ 8] K.G. Lynn, W.E. Frieze, Intense positron beams and possible experiments in "Positron scattering in Gases". J. Humberton & M.R. McDowell Ed., Nato ASI Series
- [ 9] E. Ottewitte, Large scale positron production for physics needs via fission reactors, Proceedings of the Advanced Accelerator concepts Conference Madison, WI 1986.
- [10] J. Dawson, A positron factory. Proceedings of the Workshop "Critical issues in the development of new linear colliders" Madison-Wisconsin (August 1986)
- [11] V. Balakin, A. Mikhailichenko, The conversion system for obtaining highly polarized electrons and positrons. Preprint INP 79-85 Novosibirsk
- [12] B. Kincaid, Journal of Applied Physics Vol. 48, n°7 (July 1977)
- [13] M. Sands, in "Physics with intersecting storage rings" (1971) Academic Press, B. Toushek Ed.
- [14] H. Wiedemann, SLAC Pub 2849 (November 1981)
- [15] R. Chehab, A. Nyaiesh, F. Richard, X. Artru, Study of positron source generated by photons from ultrarelativistic channeled particles. Submitted to the 1989 PAC-Chicago.
- [16] R. Helm and al., The positron source in "The Stanford two Mile Accelerator", R. Neal Editor, W.A. Benjamin Inc (1968).
- [17] J. Haïssinski, Nuclear Instruments and Methods 51 (1967) 181.
- [18] G. Stange, IEEE Trans. Nucl. Science, NS-26 n°3 (June 1979)
- [19] R. Boni, S. Guiducci, M. Vescovi, A new system for positron focusing at the Frascati Linac, LNF-81/6 (R) (1981)

- [20] R. Belbeoch and al., Rapport d'études sur le projet des linacs injecteurs de LEP (LIL), LAL PI 82-01/T, LAL Orsay
- [21] A. Enomoto and al., Proceedings of the 1986 Linac Conference, Stanford (June 1986)
- [22] R. Helm, SLAC 4, Stanford Linear Accelerator Center, Stanford (August 1962)
- [23] F. Bulos et al., IEEE Transactions on Nuclear Science, NS-32 n°5 (October 1985)  
also : J.E. Clendenin and al., SLAC Pub 4704 (September 1988)
- [24] R. Chehab and al., IEEE Transactions on Nuclear Sciences, NS-30 n°4 (August 1983)
- [25] J. Heading, An introduction to Phase Integral Methods, London : Methuen, New York : John Wiley (1962)
- [26] G.I. Silvestrov, Problems of intense secondary particle beams production, Preprint 86-163, Novosibirsk (1986)
- [27] H. Riege and al., CERN PS/87-1 (AA)
- [28] F. Amman, Positron accelerators in "Linear Accelerators" P. Lapostolle, A. Septier Editors, North-Holland Pub. Co (1970)
- [29] R. Chehab, Y. Thiery, K. Hübner, Proceedings of the 1986 Linear Accelerator Conference, June 1986, Stanford.